HHS Public Access

Author manuscript

J Mech Behav Biomed Mater. Author manuscript; available in PMC 2020 October 20.

Published in final edited form as:

J Mech Behav Biomed Mater. 2019 February ; 90: 125–132. doi:10.1016/j.jmbbm.2018.10.010.

Cortical bone properties in the Brtl/+ mouse model of Osteogenesis imperfecta as evidenced by acoustic transmission microscopy

S. Blouin[a,*], **N. Fratzl-Zelman**[a], **A. Roschger**[c], **W.A. Cabral**[b,1], **K. Klaushofer**[a], **J.C. Marini**[b], **P. Fratzl**[c], **P. Roschger**[a]

[a]Ludwig Boltzmann Institute of Osteology at the Hanusch Hospital of WGKK and AUVA Trauma Centre Meidling, 1st Medical Department Hanusch Hospital, Vienna, Austria

[b]Bone and Extracellular Matrix Branch, National Institute of Child Health and Human Development, NIH, Bethesda, MD, USA

[c]Max Planck Institute of Colloids and Interfaces, Department of Biomaterials, Postdam, Germany

Abstract

Higher skeletal fragility has been established for the Brtl/+ mouse model of osteogenesis imperfecta at the whole bone level, but previous investigations of mechanical properties at the bone material level were inconclusive. Bone material was analyzed separately at endosteal (ER) and periosteal regions (PR) on transverse femoral midshaft sections for 2-month old mice (wild-type n = 6; Brtl/+ n = 6). Quantitative backscattered electron imaging revealed that the mass density computed from mineral density maps was higher in PR than in ER for both wild-type (+2.1%, $p < 0.05$) and Brtl/+ mice (+1.8%, $p < 0.05$). Electron induced X-ray fluorescence analysis indicated significantly lower atomic Ca/P ratios and higher Na/Ca, Mg/Ca and K/Ca ratios in PR bone compared to ER independently of genotype. Second harmonic generation microscopy indicated that the occurrence of periodically alternating collagen orientation in ER of Brtl/+ mice was strongly reduced compared to wild-type mice. Scanning acoustic microscopy in time of flight mode revealed that the sound velocity and Young's modulus (estimated based on sound velocity and mass density maps) were significantly greater in PR (respectively + 6% and +15%) compared to ER in wild-type mice but not in Brtl/+ mice. ER sound velocity and Young's modulus were significantly increased in Brtl/+ mice (+9.4% and +22%, respectively) compared to wild-type mice. These data demonstrate that the *Col1a1 G349C* mutation in Brtl/+ mice affects the mechanical behavior of bone material predominantly in the endosteal region by altering the collagen orientation.

Graphical Abstract

[*]Correspondence to: Ludwig Boltzmann Institute of Osteology, UKH Meidling, Kundratstr. 37, A-1120 Vienna, Austria. stephane.blouin@osteologie.at (S. Blouin).

[1]Present Address: Molecular Genetics Section, Medical Genomics and Metabolic Genetics Branch, National Human Genome Research Institute, NIH, Bethesda, MD.

Authors' roles: All authors made substantial contributions to either the conception and design, acquisition of data or analysis and interpretation of data, participated in drafting the manuscript or revising it critically for important intellectual content, and approved the final version of the submitted manuscript.

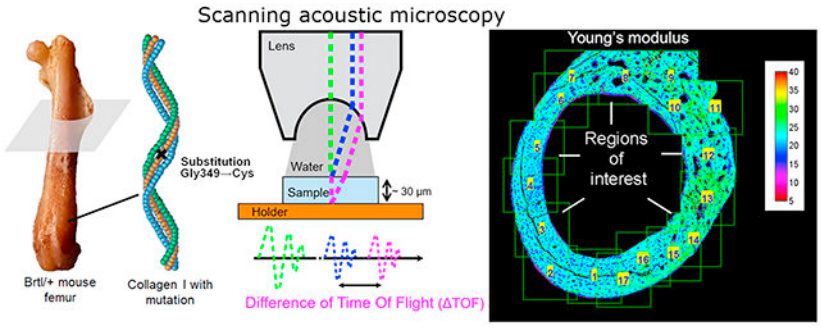

Keywords

Scanning acoustic microscopy; Sound velocities; Quantitative backscattered electron imaging; Elastic properties; Osteogenesis imperfect; Brtl/+ mice

1. Introduction

Osteogenesis imperfecta (OI) or “brittle bone disease” is a heritable disorder of connective tissues most commonly caused by *de novo* dominant mutations in the genes that encode type I collagen, *COL1A1* and *COL1A2*. Although patients present with variable findings, the defining features of OI include bone deformities, short stature, and bone fragility due to low bone mass and impaired bone material properties (Marini et al., 2017).

A general hallmark of OI bone is the hypermineralization of the bone matrix (Bishop, 2016). However, due to the scarcity of patient samples it has been difficult to investigate bone material properties in OI. While two human studies including controls evaluated the mechanical properties of OI bone material by nanoindentation, their findings were contradictory and reported either higher (Weber et al., 2006) or lower (Imbert et al., 2014) Young's modulus in bone tissue of OI patients. The majority of data has been obtained for *oim* mice, a model for Osteogenesis imperfecta in which a collagen I mutation leads to the exclusive formation of α1(I) collagen homotrimers and results in numerous phenotypic features reminiscent of OI. Changes in mineral/matrix ratio have been evidenced by Raman spectroscopy and FTIR (Bart et al., 2014; Carriero et al., 2014a; Vanleene et al., 2012; Yao et al., 2013), higher mineral content by quantitative backscattered electron imaging (qBEI) (Vanleene et al., 2012; Grabner et al., 2001; Rodriguez-Florez et al., 2014) as well as smaller and less well aligned apatite crystals (Vanleene et al., 2012; Grabner et al., 2001; Rodriguez-Florez et al., 2014; Fratzl et al., 1996), altered vascular porosity and osteocyte lacunae density (Carriero et al., 2014b) and impaired fibrillar mechanical properties (Carriero et al., 2014a). Young's modulus was found to be higher (Miller et al., 2007; Rao et al., 2008) or lower (Vanleene et al., 2012; Rodriguez-Florez et al., 2014) than controls in different studies. However, the *oim* model differs from the great majority of OI cases due to both its recessive mode of inheritance, as well as its atypical collagen I homotrimer composition. Therefore, the use of a more appropriate model may yield a better understanding of the bone matrix properties in OI.

Fewer studies have been performed on the Brtl/+ mouse, which is a heterozygous knock-in model for OI with a typical Gly349Cys substitution in one *COL1A1* allele, which was also found in a child affected by a moderately severe form of OI (type IV) (Forlino et al., 1999). Mechanical properties of whole-bone revealed reduced maximum load and work to failure in young mice (Kozloff et al., 2004; Sinder et al., 2013; Sinder et al., 2015; Uveges et al., 2009; Perosky et al., 2016). After normalization for geometric influences, a higher Young's modulus was found in femoral bones of Brtl/+ mice as compared to wild type in the age range from 8 weeks to 6 months (Kozloff et al., 2004; Sinder et al., 2013; Sinder et al., 2015; Uveges et al., 2009; Perosky et al., 2016). In addition to four-point bending, Sinder *et al.* examined the Brtl/+ periosteal bone with nanoindentation under dehydrated conditions and found a larger Young's modulus, although comparisons to wild type were not significant for any specific tissue age (Sinder et al., 2013). Interestingly, no genotype effect was detected in periosteal bone under hydrated conditions (Sinder et al., 2016).

After initial bone formation, cortical bone thickening and shaping occurs by bone apposition and resorption at both endosteal and periosteal surfaces. Differences between periostal and endosteal bone in mice have been reported recently concerning mineral (Turunen et al., 2016), material and cellular characteristics (Allen et al., 2004; Checa et al., 2015; Lee et al., 2004). Therefore, mechanical properties are potentially different between the two compartments.

The aim of the present study was to investigate bone material characteristics in long bones (femoral midshaft) of Brtl/+ mice. Periosteal and endosteal regions were examined separately to detect any compartment differences. We performed quantitative backscattered electron imaging (qBEI) to produce mineral content maps of bone tissue that were converted into bone mass density maps. The elemental composition of the bone material was investigated by electron induced X-ray fluorescence analysis (EDX) in a scanning electron microscope. In order to obtain mechanical data, we used scanning acoustic microscopy in time of flight mode (SAM-TOF) to record sound velocity maps (Blouin et al., 2014), which were combined with mass density maps to generate a corresponding Young's modulus. Since bone mechanical properties are highly dependent on collagen orientation, we also analyzed our bone samples by second harmonic generation with a confocal laser scanning microscope (Fratzl et al., 2004).

2. Material and methods

2.1. Animals

Brittle (Brtl/+, n = 6) and wild type (WT, n = 6) mice from the mixed Sv129/CD-1/C57BL/6 S background strain were euthanized at 2 months of age. Left femurs were collected and cleaned from soft tissue. The femurs were fixed in 70% ethanol immediately after removal. All protocols and procedures involving animals were conducted under an NICHD ACUC approved protocol.

2.2. Sample preparation

The sequence of sample preparation and experimental measurements is shown in a flowchart (Fig. 1). We performed one cross-section at half the length of each femur. The proximal section was dehydrated in a graded ethanol series and defatted with acetone before embedding in polymethylmethacrylate as previously described (Roschger et al., 1998). Sample blocks were trimmed using a low speed diamond saw (Isomet-R, Buehler Ltd. Lake Buff, IL, USA) to obtain transverse sections of the femoral midshaft. Sectioned bone surfaces were sequentially ground with sand paper with increasing grit size followed by polishing with diamond grains (size down to 1 μm) on hard polishing clothes by a PM5 Logitech instrument (Glasgow, Scotland). For the first run of quantitative backscattered electron imaging (qBEI) in the scanning electron microscope, the surface of the sample block was carbon coated by vacuum evaporation (Agar SEM Carbone coater; Agar Scientific Limited, Essex, UK). For Scanning acoustic microscopy in time-of-flight mode (SAM-TOF) the polished coated side of the samples already used in qBEI was glued (Technovit 7210 VLC, EXAKT, Norderstedt, Germany) to plastic slides with a precision adhesive press (EXAKT 402, EXAKT, Norderstedt, Germany). The glued blocks were cut, ground to a thickness between 25 and 35 μm, polished and carbon coated again to facilitate qBEI measurements from the second side of the sample. For more details of SAM-TOF sample preparation, see elsewhere (Blouin et al., 2014).

2.3. Quantitative backscattered electron imaging (qBEI) analyses

The details of the qBEI method have been published elsewhere (Roschger et al., 1998). Briefly, qBEI is based on the fact that the intensity of electrons backscattered from a thin surface-layer of a sectioned bone area is proportional to the weight concentration of mineral (hydroxyapatite) and thus calcium in bone. A digital scanning electron microscope (DSM 962, Zeiss, Oberkochen, Germany) was employed with an accelerating voltage of 20 kV, a working distance of 15mm and a probe current of 110 pA ± 4 pA. Backscattered electrons (BE) were measured by a four-quadrant semiconductor backscattered electron detector. Bone tissue areas were recorded with a pixel depth of 256 gray levels at a 200x nominal magnification (corresponding to a spatial resolution of 0.9 μm per pixel) using a scan speed of 100 s per frame. BE gray-levels were further converted into calcium concentration values (weight % Ca) by proper calibration and standardization as described previously (Roschger et al., 1998).

Using ImageJ software (version 1.49 g), the digital calibrated gray-level BE-images were converted in local mass density mapping using the following equation: $\rho_{bone} = 100/(HA_{wt}/\rho_{HA} + (100–HA_{wt})/\rho_{org})$, where ρ_{bone}, ρ_{HA} and ρ_{org} are the mass densities of the bone material, hydroxyapatite and organic matrix, respectively. HA_{wt} is the weight fraction of hydroxyapatite in percent and relates to the weight fraction of Calcium (wt% Ca) : HA_{wt} = 2.51×wt. %Ca (Roschger et al., 1998). The mass density of hydroxyapatite is well known (ρ_{HA} = 3.18 g/cm^3) (Skedros et al., 1993). Although it has been shown that the nanoporosity (and therefore the mass density ρ_{org}) may change in OI (Paschalis et al., 2016), we estimate that this will have only a minor effect on the calculation of the mass density of the bone material, so that the same value of ρ_{org} = 1.41 g/cm^3 (Blouin et al., 2014) is used for both OI and controls.

2.4. Quantitative energy dispersive X-ray Spectrometry (EDX)

The elemental composition was determined by quantitative Energy Dispersive X-ray Spectrometry (EDX) using a Zeiss Supra 40 field-emission scanning electron microscope (FESEM) (Zeiss, Oberkochen, Germany) equipped with a large-area (80 mm^2) EDS Silicon Drift Detector (X-Max, Oxford Instrument, United Kingdom). The analysis of the generated EDX spectra was carried out using Oxford INCA software. The FESEM was operated at 10 kV with a probe current of about 1.5 nA at 10mm working distance and an aperture size of 60 μm. A nominal magnification 4000×(28.65 nm pixel size) was used. A 29.3 μm x 22 μm observation field was continuously scanned with a speed of 3.2 μs/pixel. All spectra were acquired with an acquisition time of 30 s, a 0–10 keV spectrum range with 2000 channels and a process time of four. The systems energy canal positions were fine-tuned by acquisition of a spectrum from a highly pure Ni sample. The samples were the same as those observed by qBEI (already carbon coated). Only homogeneous bone areas (ROIs) excluding osteocyte lacunae were measured and the Ca/P, Mg/Ca, Na/Ca and K/Ca atomic ratios were determined.

2.5. Scanning acoustic microscopy in time-of-flight mode (SAM-TOF)

SAM-TOF is based on the fact that the ultrasonic velocity can be obtained by measuring a difference of time-of-flight (ΔTOF) between the ultrasonic reflection from the front and back surface of a sample with known thickness. The ultrasonic velocity is related to the mechanical material properties. Combining information of velocity and mass density enables to calculate the Young's modulus. Acoustic measurements were made with a Scanning Acoustic Microscope (SASAM®UR 1000, kibero GmbH, Saarbrücken, Germany) which consisted of an acoustic module combined with an optical upright microscope (Axio Scope. A1, Zeiss, Offenbach, Germany). A 300 MHz short pulse generator provided an ultrasound pulse of 20 ns length. A high frequency transducer (SASAM® Lens, kibero) with a semi-aperture of 30°, a working distance of 350 μm and a central frequency of 330 MHz (theoretical lateral resolution of 4.6 μm) was employed to scan in the x-y directions (320 μm x 320 μm) the sample surface in 2 μm steps and in the z direction to focus the acoustic lens on the sample surface. A drop of bidistilled water was used as inter-medium between lens and sample surface. The temperature was maintained at 23 °C ± 1 °C via the air conditioning. The signal was digitized at a rate of 8 GHz (sampling interval of 0.125 ns). The signal quality was increased by averaging 400 repeated pulse trains and removal of the background signal. The signal was analyzed with a custom-made software to obtain ΔTOF for each position of the scan. Thus we obtain a velocity mapping after determination of the local thickness with a confocal laser scanning microscope (CLSM) (Leica TCS-SP5, Leica Microsystems, Wetzlar, Germany) in reflected light mode (Fig. 1) following the procedure already published (Blouin et al., 2014). Using the sound velocity and the mass density information, the Young's modulus (E) of an isotropic and homogenous material can be calculated as:

$$E = V^2 \rho K, \quad (1)$$

with

$$K = (1 + \upsilon)^2 (1 - 2\upsilon) / (1 - \upsilon^2) \quad (2)$$

with V velocity, ρ mass density, K coefficient smaller than 1, which depends on Poisson's ratio ν only (Mavko et al., 2009). In this work, we approximate bone tissue as an isotropic material with a Poisson ratio value of 0.3 to extract E from the sound velocity.

2.6. Regions of interest for SAM and qBEI analyses

The SAM-TOF method requires a sufficient homogeneity of bone material in the size range of several micrometers. This condition was found in the circumferential lamellar bone formed at the outer and inner part of the transversal femoral midshaft section, which became the region of interest (ROI) for our measurements. These two regions were designated as periosteal (PR) and endosteal region (ER).

We excluded the central older bone area containing residuals of early bone development (woven bone and highly mineralized cartilage). This central region between ER and PR has chaotic collagen fibril orientation and is similar to what has been described by others previously in rats (Shipov et al., 2013) and mice (Ip et al., 2016) (Fig. 2). Further, zones close to sharp discontinuities within the bone area of ROI (PR and ER) which could interfere with a correct time of flight measurement or be responsible for partial void in the 30 μm thick bone section, such as canals of blood vessels, osteocyte lacunae and cracks from sample preparations, were excluded from evaluations (Blouin et al., 2014). Therefore, the entire region of the third trochanter having a high density of canals were excluded from SAM-TOF measurements (Fig. 2).

2.7. Second harmonic generation microscopy

The collagen orientation was investigated by measuring the second harmonic generated (SHG) signal of collagen in a backward direction. We used a confocal laser scanning microscope (Leica SP8 CLSM) equipped with a pulsed IR-laser tuned to a 910 nm excitation wavelength to achieve the high energies needed for a sufficient SHG signal. The signal detection was performed in the spectral window between 450 nm and 460 nm. We obtained 1024×1024 pixels images with pixel size 0.378 μm and a frame average of 8 to reduce the noise. A strong SHG signal is characteristic of regions of dense and well-aligned collagen fibrils preferentially oriented within the image plane (Chen et al., 2012; Houle et al., 2015).

2.8. Statistical analyses

Statistical analyses were carried out with the Graphpad Prism 5.0 program (GraphPad Software, Inc., La Jolla, CA, USA). Unpaired t-tests were used to compare qBEI, EDX and SAM related data between both groups. Paired t-test were used to test for within-mice differences (ER and PR comparison). Differences were considered statistically significant at $p < 0.05$. Values are presented as mean ± SD unless noted.

3. Results

The bone mass density, elemental composition, sound velocity and Young's modulus of wild-type and Brtl/+ mice were assessed separately in the periosteal (PR) and endosteal (ER) bone region of transverse femoral midshaft bone sections excluding the central woven bone and the third trochanteric region (see material and methods section). In addition, the bone sections were imaged with second harmonic generation microscopy to evaluate collagen orientation.

3.1. *Periosteal and endocortical regions appear clearly separated and differ in material composition in BOTH wild-type and Brtl/ + mice*

i. The two relatively structurally homogenous bone regions could be found in the cortical cross sections imaged by backscattered electrons irrespective of the genotype (red and yellow lines in Fig. 2A). However the cortical thickness of Brtl/+ mice appeared thinner than wild-type mice. Cartilage islands and woven bone areas clearly separate the endocortical region (ER) (yellow line) and the periosteal region (PR) (red line). This delimitation was emphasized by the observation of cracks in the woven bone/mineralized cartilage region between the ER and the PR. These cracks are caused by mechanical forces originating likely from shrinking processes due to dehydration of the tissue by resin embedding and exposure to high vacuum in the SEM. It likely denotes a discontinuity in material properties and/or a higher fragility of woven bone as compared to lamellar bone (Wagermaier et al., 2015).

ii. The distinction between ER and PR was further supported by the fact that the ER appeared darker compared to the PR in the qBEI images of both genotypes, reflecting a lower matrix mineralization in ER. The average mass density values were significantly higher in PR compared to ER in both wild-type (WT) (+2.1%, $p < 0.001$) and in Brtl/+ (+1.8%, $p < 0.05$) mice (Fig. 3A). Although there was a trend toward increased mass densities in Brtl/+ compared to wild-type for ER (+1.4%; $p = 0.061$) and PR (+1.2%; $p = 0.12$), these differences did not reach levels of significance.

iii. Such a distinction was also corroborated by the outcomes of the elemental analysis by EDX showing that the Ca/P atomic ratio was significantly lower, while Na/Ca, Mg/Ca and K/Ca ratios were significantly higher in PR compared to ER for both genotypes (see Table 1).

iv. The second harmonic generation imaging showed random collagen orientation in the central region containing woven bone and cartilage islands for both wild-type and Brtl/+ mice, confirming the distinction between ER and PR. In PR, a similar periodically alternating collagen orientation was visible for both groups (Fig. 4). However, in the ER this characteristic pattern appeared similar or slightly enhanced compared to PR in wild type mice, whereas the SHG signal was almost absent in ER of Brtl/+ mice (Fig. 4).

3.2. *Abolition of mechanical differences between ER and PR in Brtl/+ mice*

The combination of sound velocity maps with mass density maps of ER and PR (Fig. 5) lead to the following outcomes (Fig. 3B and C):

- **i.** overall, the sound velocity was in the range of 3750–4100 m/s and the Young's modulus in the range of 24–30 GPa.
- **ii.** in wild-type mice sound velocity and Young's modulus were increased (+6.0% and +15.1%, $p < 0.05$, respectively) in PR with respect to ER.
- **iii.** In Brtl/+ mice no significant differences of sound velocity and Young's modulus between ER and PR could be observed.
- **iv.** The sound velocity and Young's modulus of Brtl/+ in ER were significantly increased (+9.4% and +21.4%, $p < 0.05$, respectively) compared to that in wild-type.

4. Discussion

The present work addresses the elastic characteristics of bone in the Brtl/+ mouse, a model for moderately severe OI (type IV). We took advantage of high spatial resolution methods to investigate the bone material level at microscale. Our findings demonstrate that bone material originating from the periosteal region (PR) has a higher mass density, a higher Ca/P and lower Na/Ca, Mg/Ca, K/Ca ratios, than that at the endosteal region (ER) in both wild-type and Brtl/+ mice. However, there was a tendency for higher overall mass density in Brtl/+ mice. The most striking result was the absence of any difference in sound velocity and Young's modulus in Brtl/+ between the ER and PR, although the mass density values were significantly different. The observation of collagen orientation disturbance in ER of Brtl/+ mice provided an explanation for this mechanical finding.

Independent of the difference in cortical thickness between both genotypes found in this study and previous descriptions (Kozloff et al., 2004), it was crucial for to discriminate similarly between periosteal (PR) and endocortical (ER) bone regions for both genotypes. Interestingly, the PR was more highly mineralized than the ER for both genotypes. Further, differences in the elemental composition were found between these regions independently of the genotype. In contrast, low Ca/P ratios have been reported in OI patients compared to healthy individuals (Cassella et al., 1995; Sarathchandra et al., 1999). Furthermore, conflicting Ca/P ratio results have been reported in *oim* mice using non-spatially resolved methods on whole bone (Camacho et al., 1999; Carleton et al., 2008; Phillips et al., 2000). According to our spatially resolved EDX measurements, the Ca/P ratio was similar in Brtl/+ and wild type mice, but the Ca/P ratio was always lower in the PR than in the ER in both genotypes. On the other hand, the elemental fraction of Mg, K and Na was increased in PR. We speculate that one reason for these differences is that the microenvironment at endosteal and periosteal surfaces are not identical. For instance, local mechanical stresses on the ER and PR may not be the same. Furthermore, consistent with reports that osteoblastic protein expression differs in endosteal and periosteal compartments, cellular activity in these two bone compartments may vary (Allen et al., 2004; Simsek Kiper et al., 2016). The collagen organization is distinct between both compartments (Kerschnitzki et al., 2011). There is

some evidence that mineralization process, hydroxyapatite crystal size or mineral apposition rate are different between both bone compartments in murine animals (Turunen et al., 2016; Checa et al., 2015; Lee et al., 2004; Hassler et al., 2014). Taken together, these observations support our qBEI and EDX findings of differences between ER and PR bone material.

The mechanical properties that were assessed by SAM-TOF revealed distinct values of Young's modulus in the ER (23.8 GPa) and PR (27.4 GPa) of wild-type mice, coinciding with an increasing mass density (ER: 2244 kg/m^3; PR: 2291 kg/m^3) and consistent with a common positive correlation found between mineral content / mass density and material stiffness / Young's modulus (Currey, 1988). However, two arguments suggest that other factors beyond mineral content might influence the mechanical findings: 1) it is unlikely that a 2% mass density difference accounts for a 15% elastic modulus difference between ER and PR in wild-type mice. A 7% elastic modulus difference would be more reliable based on the relationship between mass density and elastic modulus in human osteonal samples (Blouin et al., 2014). 2) Young's moduli in Brtl/+ mice were not different between ER (28.9 GPa) and PR (29.1 GPa) despite the differences in their mass densities (ER: 2275 kg/m^3; PR: 2318 kg/m^3). A potential factor for these inconstancies is the collagen fibril orientation with respect to the direction of loading/deformation (Fratzl et al., 2004; Wagermaier et al., 2015) which has an impact on the mechanical test outcomes. Indeed our observation with second harmonic generation, suggesting an enhanced in-plane orientation in ER compared to PR in wild-type mice is in line with the important elastic modulus difference found. In contrast, the absent or weak second harmonic signal found in ER of Brtl/+ indicates an enhanced out of plane orientation compared to PR, and thus is in agreement with the finding of similar elastic properties in spite of different mass density. Interestingly, alterations of collagen fibril orientation observed by polarized light were also reported in mov13 mice (Jepsen et al., 1997), an OI mouse model of a quantitative collagen I defect, and in *oim* mice (Chipman et al., 1993). Increased variability of collagen fibril orientation in *oim* mice was previously demonstrated by measuring the degree of alignment of the mineral crystal reflecting the fibril orientation by small angle X-ray scattering (Fratzl et al., 1996). These observations of a less organized collagen fibril orientation in OI animal models are in line with the characteristic clinical finding of various altered lamellar phenotype depending on the OI type (Rauch and Glorieux, 2004).

In a prior report on the mechanical properties of Brtl/+ bone, a trend toward higher tissue Young's modulus was observed by nanoindentation at well-defined tissue ages (Sinder et al., 2013). For instance, the elastic modulus in Brtl/+ mice was 28 GPa in 7-day-old bone compared to 26 GPa in wild-type mice, without distinction between endosteal or periosteal compartments. At the same tissue age (7 days), a second nanoindentation study performed in a hydration chamber revealed an elastic modulus of 10 GPa for both wildtype and Brtl/+ mice in growing and adult murine periosteal bone (Sinder et al., 2016). Although this value varies from our experiment, the finding of no difference between wild-type and Brtl/+ mice is in agreement with our findings in PR. In contrast, whole bone three- or four-point bending tests revealed significantly higher Young's moduli at different ages in Brtl/+ compared to wild-type mice of the same age (Kozloff et al., 2004; Sinder et al., 2013; Sinder et al., 2015; Uveges et al., 2009), with a range from several hundred MPa up to several GPa.

In general, there is a large variation of the Young's modulus values reported on the bone material of OI murine models and OI patients. The Young's modulus obtained by 3 point bending was found to be higher (Miller et al., 2007; Rao et al., 2008; Misof et al., 2005) or similar (Bart et al., 2014; Yao et al., 2013) in bone of *oim* compared to wild-type mice (in the range from 1 to 10 GPa). Two nanoindentation experiments with different settings reported an average Young's modulus lower in dry bone of *oim* mice (34 GPa or 12 GPa respectively) compared to wild-type (42 GPa or 15 GPa respectively) (Vanleene et al., 2012; Rodriguez-Florez et al., 2014) without distinguishing the bone compartments. In transiliac bone biopsy samples from patients with mild to severe forms of OI (type I, IV and III), the Young's modulus obtained in cortical and trabecular bone by nanoindentation were in the range between 16 and 21 GPa (Weber et al., 2006; Albert et al., 2013; Fan et al., 2007). Nevertheless it remains controversial whether the Young's modulus is increased or decreased compared to age-matched controls (Weber et al., 2006; Imbert et al., 2014).

Several factors should be considered for the large variation in the Young's modulus outcomes in the literature:

i. the type of mechanical testing. The material properties in three or four-point bending experiments are derived from whole bone properties (combination of endosteal and periosteal bone and an unknown portion of cartilage) by taking into account the geometry of the bone. However bone does not have standardized shape as required by beam theory which might lead to underestimation of the Young's modulus by a factor of 2 or more compared to nanoindentation or micro-finite element analysis (Silva et al., 2004; van Lenthe et al., 2008). In contrast, nanoindentation directly tests the mechanical properties at a material level yet variations in outcome are reported depending on the indenter geometry and the analysis method (Rodriguez-Florez et al., 2013). The acoustic method used in this work is also a direct measure of the bone material. However, the overall Young's modulus values were some-what higher (almost 30 GPa) than those obtained by nanoindentation (range between 10 and 20 GPa). This is likely due to differences of deformation rate between the two methods. While nanoindentation is a quasi-static method, scanning acoustic microscopy generates a dynamic strain by using ultrasound frequency reaching hundreds of MHz and inducing viscoelastic phenomena responsible for the higher value of elastic modulus. Rupin *et al.* reported nearly doubled values of the acoustic Young's modulus at 200 MHz compared to nanoindentation-acquired Young's modulus (Rupin et al., 2009). Nevertheless, nanoindentation and SAM-TOF techniques provided highly correlated data indicating that they mirror relatively similar differences in mechanical properties of samples.

ii. the anatomical site of measurements within the bone sample, e.g. the discrimination between periosteal and endosteal regions, as shown in this study and the local tissue age, allow a more detailed bone characterization compared to bulk measurements.

iii. the material condition at the time of measurement. The Young's modulus is dependent on whether the sample is dehydrated, hydrated, native, resin-

embedded or rehydrated (physiological sodium solution or Hanks balanced salt solution) (Bembey et al., 2006; Gustafson et al., 1996).

iv. the underlying mutations causing OI might hamper collagen synthesis and fibrillogenesis in different manners and to various extents.

There are several limitations to the current study. First, we focused only on two month-old Brtl/+ mice. Evolution of the mineral and mechanical properties at material level over a range of ages could be of interest to investigate, as they may change over time. Indeed, adaptations in cortical thickness and a drift of the bone regions during bone growth is noticeable due to changes in the ratio of endosteal and periosteal bone formation. Second, while the sound velocity data are the directly measured physical variable, the Young's modulus is derived using a formula with a constant Poisson's ratio of 0.3 which might affect the results (Blouin et al., 2014). Further, it was assumed that bone material is isotropic and homogeneous. The collagen fibril arrangement is known to induce a strong anisotropy into the bone material. We also presumed that bone mineral is pure hydroxyapatite with a density of 3.18 g/cm^3 and a Ca/P atomic ratio of 1.67, but our EDX elemental analysis revealed a Ca/P value of about 1.52. By calculation, as shown elsewhere (Roschger et al., 2014), mass density would be underestimated by 0.13% compared to pure hydroxyapatite at 25 wt% Ca as measured by qBEI. In addition, the assumption of unchanged organic matrix density between wild-type and Brtl/+ mice may not be fully accurate as hydration of collagen fibrils has been found reduced in the oim mouse model of osteogenesis imperfecta (Andriotis et al., 2015). The impact of hydration on the mineralization process is unknown. However it is likely that the difference in fibrils hydration together with the increased mineral content in OI might further contribute to the brittleness (Bertinetti et al., 2015). Another limitation was that possible differences in mineralization kinetics / processes between ER and PR could not be examined due to the absence of fluorochrome administration for bone labeling.

In conclusion, we showed with high spatial resolution methods that the collagen mutation in Brtl/+ mice affects the mechanical behavior of femoral bone material predominantly in the endosteal region. We suggest that the less organized collagen fiber orientation is the major contributor to the altered overall stiffness and, therefore, to the deterioration of mechanical competence in this OI mouse model. These data are further evidence that the fragility observed in OI patients is not only due to low bone mass but also to bone material alterations that modify its mechanical properties.

Acknowledgements

We thank Sonja Lueger, Daniela Gabriel, Petra Keplinger and Phaedra Messmer for excellent technical assistance at the bone material laboratory of the Ludwig Boltzmann Institute of Osteology, Vienna, Austria. This study was supported by the Allgemeine Unfallversicherungsanstalt (AUVA), research funds of the Austrian workers compensation board, Austria, and the Wiener Gebietskrankenkasse (WGKK), Vienna Regional Health Insurance Fund, Austria. JCM received the grant Z01-HD0008830-01 from NICHD, NIH, USA intramural funding.

References

Albert C, Jameson J, Toth JM, Smith P, Harris G, 2013 Bone properties by nanoindentation in mild and severe osteogenesis imperfecta. Clin. Biomech 28 (1), 110–116.

Allen MR, Hock JM, Burr DB, 2004 Periosteum: biology, regulation, and response to osteoporosis therapies. Bone 35 (5), 1003–1012. [PubMed: 15542024]

Andriotis OG, Chang SW, Vanleene M, Howarth PH, Davies DE, Shefelbine SJ, Buehler MJ, Thurner PJ, 2015 Structure-mechanics relationships of collagen fibrils in the osteogenesis imperfecta mouse model. J. R. Soc., Interface / R. Soc 12 (111), 20150701.

Bart ZR, Hammond MA, Wallace JM, 2014 Multi-scale analysis of bone chemistry, morphology and mechanics in the oim model of osteogenesis imperfecta. Connect. Tissue Res 55 (Suppl 1), 4–8. [PubMed: 25158170]

Bembey AK, Bushby AJ, Boyde A, Ferguson VL, Oyen ML, 2006 Hydration effects on the micro-mechanical properties of bone. J. Mater. Res 21 (08), 1962–1968.

Bertinetti L, Masic A, Schuetz R, Barbetta A, Seidt B, Wagermaier W, Fratzl P, 2015 Osmotically driven tensile stress in collagen-based mineralized tissues. J. Mech. Behav. Biomed. Mater 52, 14–21. [PubMed: 25862347]

Bishop N, 2016 Bone material properties in osteogenesis imperfecta. J. Bone Mineral. Res. : Off. J. Am. Soc. Bone Mineral. Res 31 (4), 699–708.

Blouin S, Puchegger S, Roschger A, Berzlanovich A, Fratzl P, Klaushofer K, Roschger P, 2014 Mapping dynamical mechanical properties of osteonal bone by scanning acoustic microscopy in time-of-flight mode, Microscopy and microanalysis: the official journal of Microscopy Society of America. Microbe. Anal. Soc., Microsc. Soc. Can 20 (3), 924–936.

Camacho NP, Hou L, Toledano TR, Ilg WA, Brayton CF, Raggio CL, Root L, Boskey AL, 1999 The material basis for reduced mechanical properties in oim mice bones. J. Bone Mineral. Res. : Off. J. Am. Soc. Bone Mineral. Res 14 (2), 264–272.

Carleton SM, McBride DJ, Carson WL, Huntington CE, Twenter KL, Rolwes KM, Winkelmann CT, Morris JS, Taylor JF, Phillips CL, 2008 Role of genetic background in determining phenotypic severity throughout postnatal development and at peak bone mass in Col1a2 deficient mice (oim). Bone 42 (4), 681–694. [PubMed: 18313376]

Carriero A, Doube M, Vogt M, Busse B, Zustin J, Levchuk A, Schneider P, Muller R, Shefelbine SJ, 2014b Altered lacunar and vascular porosity in osteogenesis imperfecta mouse bone as revealed by synchrotron tomography contributes to bone fragility. Bone 61, 116–124. [PubMed: 24373921]

Carriero A, Zimmermann EA, Paluszny A, Tang SY, Bale H, Busse B, Alliston T, Kazakia G, Ritchie RO, Shefelbine SJ, 2014a How tough is brittle bone? Investigating osteogenesis imperfecta in mouse bone. J. Bone Mineral. Res. : Off. J. Am. Soc. Bone Mineral. Res 29 (6), 1392–1401.

Cassella JP, Garrington N, Stamp TC, Ali SY, 1995 An electron probe X-ray microanalytical study of bone mineral in osteogenesis imperfecta. Calcif. Tissue Int 56 (2), 118–122. [PubMed: 7736319]

Checa S, Hesse B, Roschger P, Aido M, Duda GN, Raum K, Willie BM, 2015 Skeletal maturation substantially affects elastic tissue properties in the endosteal and periosteal regions of loaded mice tibiae. Acta Biomater. 21, 154–164. [PubMed: 25900443]

Chen X, Nadiarynkh O, Plotnikov S, Campagnola PJ, 2012 Second harmonic generation microscopy for quantitative analysis of collagen fibrillar structure. Nat. Protoc 7 (4), 654–669. [PubMed: 22402635]

Chipman SD, Sweet HO, McBride DJ Jr., Davisson MT, Marks SC Jr., Shuldiner AR, Wenstrup RJ, Rowe DW, Shapiro JR, 1993 Defective pro alpha 2(I) collagen synthesis in a recessive mutation in mice: a model of human osteogenesis imperfecta. Proc. Natl. Acad. Sci. USA 90 (5), 1701–1705. [PubMed: 8446583]

Currey JD, 1988 The effect of porosity and mineral content on the Young's modulus of elasticity of compact bone. J. Biomech 21 (2), 131–139. [PubMed: 3350827]

Fan Z, Smith PA, Harris GF, Rauch F, Bajorunaite R, 2007 Comparison of nanoindentation measurements between osteogenesis imperfecta Type III and Type IV and between different anatomic locations (femur/tibia versus iliac crest). Connect. Tissue Res 48 (2), 70–75. [PubMed: 17453908]

Forlino A, Porter FD, Lee EJ, Westphal H, Marini JC, 1999 Use of the Cre/lox recombination system to develop a non-lethal knock-in murine model for osteogenesis imperfecta with analpha1(I) G349C substitution. variability in phenotype in BrtlIV mice. J. Biol. Chem 274 (53), 37923–37931. [PubMed: 10608859]

Fratzl P, Paris O, Klaushofer K, Landis WJ, 1996 Bone mineralization in an osteogenesis imperfecta mouse model studied by small-angle x-ray scattering. J. Clin. Investig 97 (2), 396–402. [PubMed: 8567960]

Fratzl P, Gupta HS, Paschalis EP, Roschger P, 2004 Structure and mechanical quality of the collagen-mineral nano-composite in bone. J. Mater. Chem 14 (14), 2115–2123.

Grabner B, Landis WJ, Roschger P, Rinnerthaler S, Peterlik H, Klaushofer K, Fratzl P, 2001 Age- and genotype-dependence of bone material properties in the osteogenesis imperfecta murine model (oim). Bone 29 (5), 453–457. [PubMed: 11704498]

Gustafson MB, Martin RB, Gibson V, Storms DH, Stover SM, Gibeling J, Griffin L, 1996 Calcium buffering is required to maintain bone stiffness in saline solution. J. Biomech 29 (9), 1191–1194. [PubMed: 8872276]

Hassler N, Roschger A, Gamsjaeger S, Kramer I, Lueger S, van Lierop A, Roschger P, Klaushofer K, Paschalis EP, Kneissel M, Papapoulos S, 2014 Sclerostin deficiency is linked to altered bone composition. J. Bone Mineral. Res 29 (10), 2144–2151.

Houle MA, Couture CA, Bancelin S, Van der Kolk J, Auger E, Brown C, Popov K, Ramunno L, Legare F, 2015 Analysis of forward and backward second harmonic generation images to probe the nanoscale structure of collagen within bone and cartilage. J. Biophotonics 8 (11–12), 993–1001. [PubMed: 26349534]

Imbert L, Auregan JC, Pernelle K, Hoc T, 2014 Mechanical and mineral properties of osteogenesis imperfecta human bones at the tissue level. Bone 65, 18–24. [PubMed: 24803077]

Ip V, Toth Z, Chibnall J, McBride-Gagyi S, 2016 Remnant woven bone and calcified cartilage in mouse bone: differences between ages/sex and effects on bone strength. PloS One 11 (11), e0166476. [PubMed: 27829059]

Jepsen KJ, Schaffler MB, Kuhn JL, Goulet RW, Bonadio J, Goldstein SA, 1997 Type I collagen mutation alters the strength and fatigue behavior of Mov13 cortical tissue. J. Biomech 30 (11–12), 1141–1147. [PubMed: 9456382]

Kerschnitzki M, Wagermaier W, Roschger P, Seto J, Shahar R, Duda GN, Mundlos S, Fratzl P, 2011 The organization of the osteocyte network mirrors the extracellular matrix orientation in bone. J. Struct. Biol 173 (2), 303–311. [PubMed: 21081167]

Kozloff KM, Carden A, Bergwitz C, Forlino A, Uveges TE, Morris MD, Marini JC, Goldstein SA, 2004 Brittle IV mouse model for osteogenesis imperfecta IV demonstrates postpubertal adaptations to improve whole bone strength. J. Bone Mineral. Res. : Off. J. Am. Soc. Bone Mineral. Res 19 (4), 614–622.

Lee K, Jessop H, Suswillo R, Zaman G, Lanyon L, 2004 The adaptive response of bone to mechanical loading in female transgenic mice is deficient in the absence of oestrogen receptor-alpha and -beta. J. Endocrinol 182 (2), 193–201. [PubMed: 15283680]

Marini JC, Forlino A, Bachinger HP, Bishop NJ, Byers PH, Paepe A, Fassier F, Fratzl-Zelman N, Kozloff KM, Krakow D, Montpetit K, Semler O, 2017 Osteogenesis imperfecta. Nat. Rev. Dis. Prim 3, 17052. [PubMed: 28820180]

Mavko G, Mukerji T, Dvorkin J, 2009 The rock physics handbook : tools for seismic analysis of porous media, 2nd ed. Cambridge University Press, Cambridge, UK ; New York.

Miller E, Delos D, Baldini T, Wright TM, Pleshko Camacho N, 2007 Abnormal mineral-matrix interactions are a significant contributor to fragility in oim/oim bone. Calcif. Tissue Int 81 (3), 206–214. [PubMed: 17660935]

Misof BM, Roschger P, Baldini T, Raggio CL, Zraick V, Root L, Boskey AL, Klaushofer K, Fratzl P, Camacho NP, 2005 Differential effects of alendronate treatment on bone from growing osteogenesis imperfecta and wild-type mouse. Bone 36 (1), 150–158. [PubMed: 15664013]

Paschalis EP, Gamsjaeger S, Fratzl-Zelman N, Roschger P, Masic A, Brozek W, Hassler N, Glorieux FH, Rauch F, Klaushofer K, Fratzl P, 2016 Evidence for a Role for Nanoporosity and Pyridinoline Content in Human Mild Osteogenesis Imperfecta. J. Bone Mineral. Res. : Off. J. Am. Soc. Bone Mineral. Res 31 (5), 1050–1059.

Perosky JE, Khoury BM, Jenks TN, Ward FS, Cortright K, Meyer B, Barton DK, Sinder BP, Marini JC, Caird MS, Kozloff KM, 2016 Single dose of bisphosphonate preserves gains in bone mass

following cessation of sclerostin antibody in Brtl/+ osteogenesis imperfecta model. Bone 93, 79–85. [PubMed: 27641475]

Phillips CL, Bradley DA, Schlotzhauer CL, Bergfeld M, Libreros-Minotta C, Gawenis LR, Morris JS, Clarke LL, Hillman LS, 2000 Oim mice exhibit altered femur and incisor mineral composition and decreased bone mineral density. Bone 27 (2), 219–226. [PubMed: 10913914]

Rao SH, Evans KD, Oberbauer AM, Martin RB, 2008 Bisphosphonate treatment in the oim mouse model alters bone modeling during growth. J. Biomech 41 (16), 3371–3376. [PubMed: 19022450]

Rauch F, Glorieux FH, 2004 Osteogenesis imperfecta. Lancet 363 (9418), 1377–1385. [PubMed: 15110498]

Rodriguez-Florez N, Oyen ML, Shefelbine SJ, 2013 Insight into differences in nanoindentation properties of bone. J. Mech. Behav. Biomed. Mater 18, 90–99. [PubMed: 23262307]

Rodriguez-Florez N, Garcia-Tunon E, Mukadam Q, Saiz E, Oldknow KJ, Farquharson C, Millan JL, Boyde A, Shefelbine SJ, 2014 An investigation of the mineral in ductile and brittle cortical mouse bone. J. Bone Mineral. Res. : Off. J. Am. Soc. Bone Mineral. Res

Roschger A, Gamsjaeger S, Hofstetter B, Masic A, Blouin S, Messmer P, Berzlanovich A, Paschalis EP, Roschger P, Klaushofer K, Fratzl P, 2014 Relationship between the v(2)PO(4)/amide III ratio assessed by Raman spectroscopy and the calcium content measured by quantitative backscattered electron microscopy in healthy human osteonal bone. J. Biomed. Opt 19 (6), 065002. [PubMed: 24919447]

Roschger P, Fratzl P, Eschberger J, Klaushofer K, 1998 Validation of quantitative backscattered electron imaging for the measurement of mineral density distribution in human bone biopsies. Bone 23 (4), 319–326. [PubMed: 9763143]

Rupin F, Saied A, Dalmas D, Peyrin F, Haupert S, Raum K, Barthel E, Boivin G, Laugier P, 2009 Assessment of microelastic properties of bone using scanning acoustic microscopy: a face-to-face comparison with nanoindentation. Jpn J. Appl. Phys 48, 07GK01.

Sarathchandra P, Kayser MV, Ali SY, 1999 Abnormal mineral composition of osteogenesis imperfecta bone as determined by electron probe X-ray microanalysis on conventional and cryosections. Calcif. Tissue Int 65 (1), 11–15. [PubMed: 10369727]

Shipov A, Zaslansky P, Riesemeier H, Segev G, Atkins A, Shahar R, 2013 Unremodeled endochondral bone is a major architectural component of the cortical bone of the rat (Rattus norvegicus). J. Struct. Biol 183 (2), 132–140. [PubMed: 23643909]

Silva MJ, Brodt MD, Fan Z, Rho JY, 2004 Nanoindentation and whole-bone bending estimates of material properties in bones from the senescence accelerated mouse SAMP6. J. Biomech 37 (11), 1639–1646. [PubMed: 15388305]

Simsek Kiper PO, Saito H, Gori F, Unger S, Hesse E, Yamana K, Kiviranta R, Solban N, Liu J, Brommage R, Boduroglu K, Bonafe L, Campos-Xavier B, Dikoglu E, Eastell R, Gossiel F, Harshman K, Nishimura G, Girisha KM, Stevenson BJ, Takita H, Rivolta C, Superti-Furga A, Baron R, 2016 Cortical-bone fragility-insights from sFRP4 deficiency in Pyle's disease. New Engl. J. Med 374 (26), 2553–2562. [PubMed: 27355534]

Sinder BP, Eddy MM, Ominsky MS, Caird MS, Marini JC, Kozloff KM, 2013 Sclerostin antibody improves skeletal parameters in a Brtl/+ mouse model of osteogenesis imperfecta. J. Bone Mineral. Res. : Off. J. Am. Soc. Bone Mineral. Res 28 (1), 73–80.

Sinder BP, Salemi JD, Ominsky MS, Caird MS, Marini JC, Kozloff KM, 2015 Rapidly growing Brtl/+ mouse model of osteogenesis imperfecta improves bone mass and strength with sclerostin antibody treatment. Bone 71, 115–123. [PubMed: 25445450]

Sinder BP, Lloyd WR, Salemi JD, Marini JC, Caird MS, Morris MD, Kozloff KM, 2016 Effect of anti-sclerostin therapy and osteogenesis imperfecta on tissue-level properties in growing and adult mice while controlling for tissue age. Bone 84, 222–229. [PubMed: 26769006]

Skedros JG, Bloebaum RD, Bachus KN, Boyce TM, Constantz B, 1993 Influence of mineral content and composition on graylevels in backscattered electron images of bone. J. Biomed. Mater. Res 27 (1), 57–64. [PubMed: 8420999]

Turunen MJ, Kaspersen JD, Olsson U, Guizar-Sicairos M, Bech M, Schaff F, Tagil M, Jurvelin JS, Isaksson H, 2016 Bone mineral crystal size and organization vary across mature rat bone cortex. J. Struct. Biol 195 (3), 337–344. [PubMed: 27417019]

Uveges TE, Kozloff KM, Ty JM, Ledgard F, Raggio CL, Gronowicz G, Goldstein SA, Marini JC, 2009 Alendronate treatment of the brtl osteogenesis imperfecta mouse improves femoral geometry and load response before fracture but decreases predicted material properties and has detrimental effects on osteoblasts and bone formation. J. Bone Mineral. Res. : Off. J. Am. Soc. Bone Mineral. Res 24 (5), 849–859.

Van Lenthe GH, Voide R, Boyd SK, Muller R, 2008 Tissue modulus calculated from beam theory is biased by bone size and geometry: implications for the use of three-point bending tests to determine bone tissue modulus. Bone 43 (4), 717–723. [PubMed: 18639658]

Vanleene M, Porter A, Guillot PV, Boyde A, Oyen M, Shefelbine S, 2012 Ultra-structural defects cause low bone matrix stiffness despite high mineralization in osteogenesis imperfecta mice. Bone 50 (6), 1317–1323. [PubMed: 22449447]

Wagermaier W, Klaushofer K, Fratzl P, 2015 Fragility of bone material controlled by internal interfaces. Calcif. Tissue Int 97 (3), 201–212. [PubMed: 25772807]

Weber M, Roschger P, Fratzl-Zelman N, Schoberl T, Rauch F, Glorieux FH, Fratzl P, Klaushofer K, 2006 Pamidronate does not adversely affect bone intrinsic material properties in children with osteogenesis imperfecta. Bone 39 (3), 616–622. [PubMed: 16644299]

Yao X, Carleton SM, Kettle AD, Melander J, Phillips CL, Wang Y, 2013 Gender-dependence of bone structure and properties in adult osteogenesis imperfecta murine model. Ann. Biomed. Eng 41 (6), 1139–1149. [PubMed: 23536112]

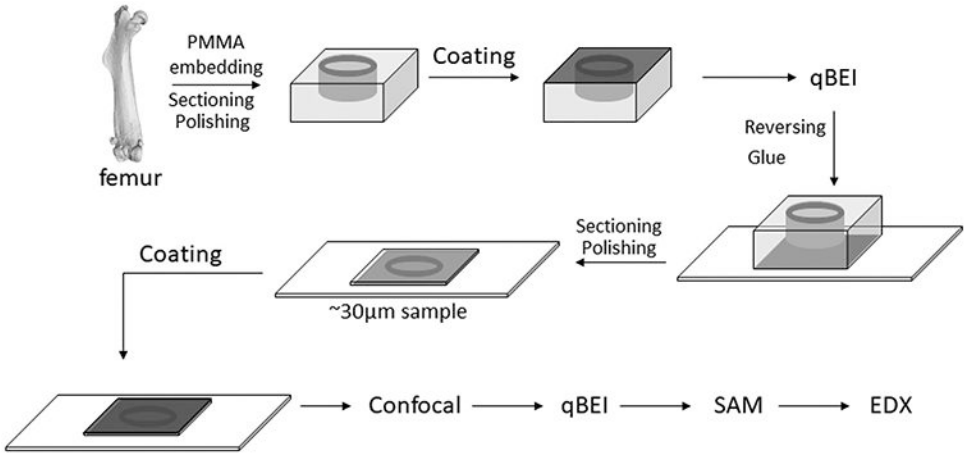

Fig. 1.

Flowchart showing the different preparation and measurement steps of a sample during this study.

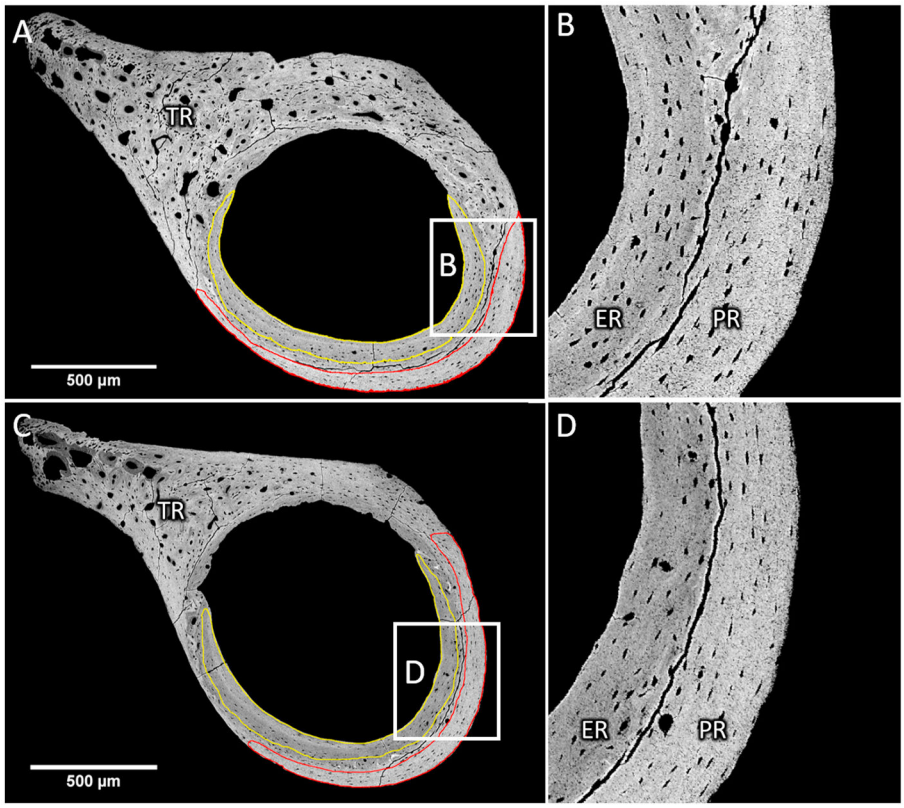

Fig. 2.

Femoral cross-sections of wild-type (A, B) and Brtl/+ (C, D) mice. Typical delimitation of endocortical (ER) and periosteal (PR) bone observed on a qBEI picture with high contrast at low (A, C) and high (B, D) magnification. The cortical thickness in Brtl/+ mice is smaller than in wild-type mice. ER and PR are separated by remnants of cartilage tissue resulting from the early phase of bone development. Noteworthy are the cracks due to sample preparation followed the delimitation. The third trochanter (TR) was excluded from the measurement since it exhibits a high porosity, high mineralization heterogeneity and numerous cartilage remnants.

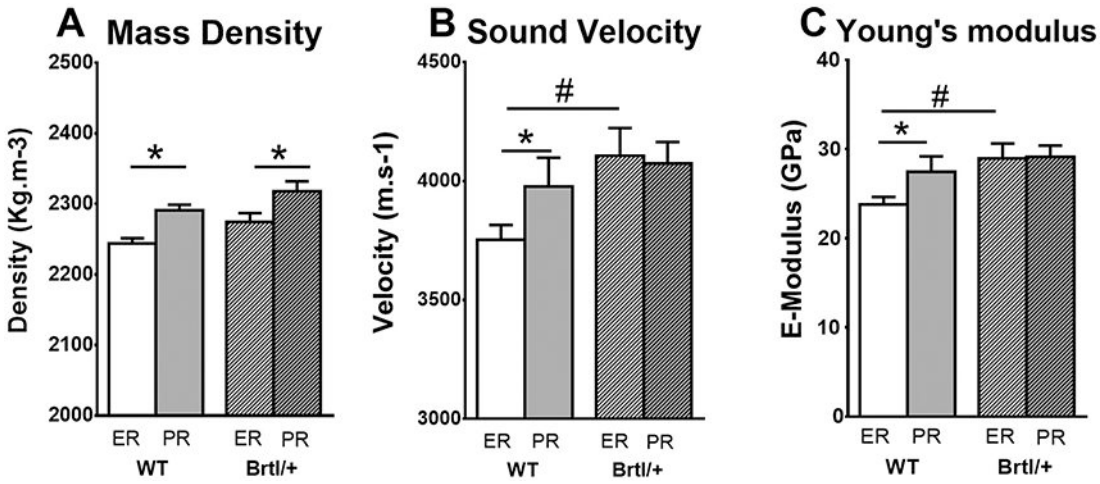

Fig. 3.

Bar chart showing (A) mass density, (B) sound velocity and (C) estimated Young's modulus in endocortical (white) and periosteal (gray) region of wild-type (no filling) and Brtl/+ (stripes) mice. While wild-type mice exhibit density, velocity and Young's modulus differences between endocortical and periosteal region, Brtl/+ mice show only differences in mass density but not in sound velocity and Young's modulus. Moreover the sound velocity and the Young's modulus in endocortical region of Brtl/+ mice was significantly higher than in wild-type. * $p < 0.05$ vs endocortical of same group. $^{\#}$ $p < 0.05$ vs same region in wild-type mice.

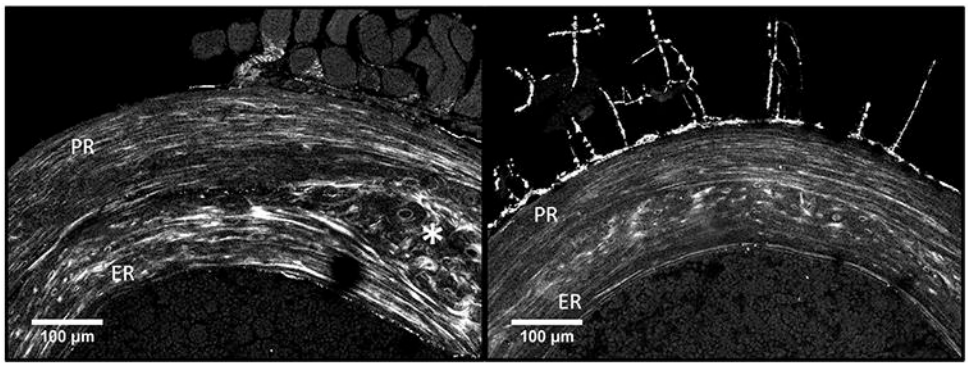

Fig. 4.

Second harmonic generation (SHG) imaging from mouse femoral cross-section. (left) wild-type: the SHG signal is stronger in endocortical region (ER) than in periosteal region (PR) denoting an enhanced in-plane orientation of the collagen fibers. Noteworthy is the woven bone region (*) separating ER and PR arising from the early phase of bone development. (right) Brtl/+ : weak SHG signal in ER compared to PR indicating an increased out-of-plane orientation of the collagen fibers.

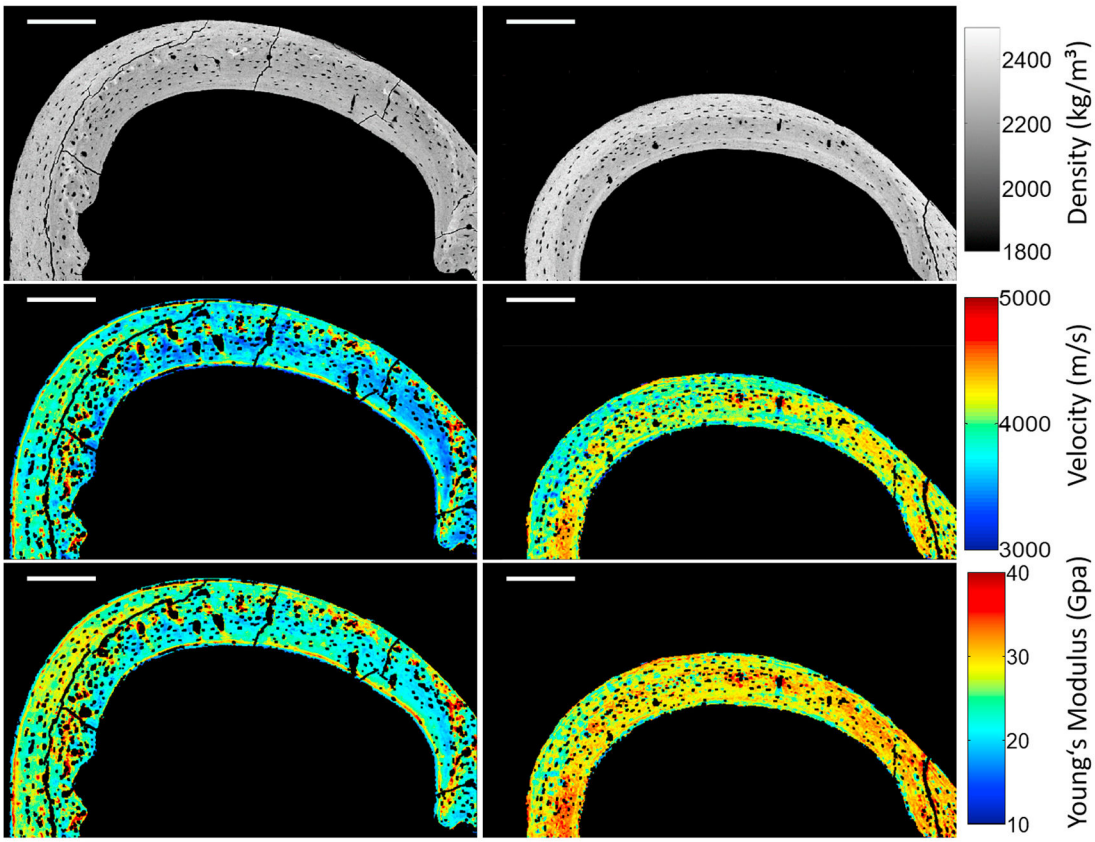

Fig. 5.

Example of the combination of mass density mapping derived from qBEI images (first row) with velocity mapping acquired with SAM (second row) to obtain the Young's modulus mapping (third row) on a femoral cross-section of WT (left column) and Brtl/+ (right column) mice. Scale bar = 200 μm.

Table 1

Elemental composition obtained by Quantitative Energy Dispersive X-ray Spectrometry.

Ratios	Wild-type (mean ± SD)			Brtl/+ (mean ± SD)		
	ER	PR	Δ (%)	ER	PR	Δ (%)
Ca/P	1.527 ± 0.0097	1.512 ± 0.0065	− 0.96 *	1.529 ± 0.0114	1.512 ± 0.0095	− 1.07 *
Na/Ca	0.041 ± 0.0027	0.05 ± 0.0017	21.68 * *	0.042 ± 0.0023	0.049 ± 0.004	16.2 *
Mg/Ca	0.027 ± 0.0004	0.03 ± 0.0014	10.64 * *	0.027 ± 0.001	0.029 ± 0.0008	9.17 * *
K/Ca	0.006 ± 0.0017	0.008 ± 0.0012	33.2 * *	0.006 ± 0.0012	0.008 ± 0.0016	24.73 *

Significant elemental ratio differences were found between endocortical (ER) and periosteal (PR) region in both wild-type and Brtl/+ mice but not between these both groups.

* $p < 0.05$ vs ER

* * $p < 0.01$ vs ER

* * $p < 0.001$.